Science Advances

AAAS

advances.sciencemag.org/cgi/content/full/2/4/e1501914/DC1

Supplementary Materials for

A checkpoint control orchestrates the replication of the two chromosomes of *Vibrio cholerae*

Marie-Eve Val, Martial Marbouty, Francisco de Lemos Martins, Sean P. Kennedy, Harry Kemble, Michael J. Bland, Christophe Possoz, Romain Koszul, Ole Skovgaard, Didier Mazel

Published 22 April 2016, *Sci. Adv.* **2**, e1501914 (2016)
DOI: 10.1126/sciadv.1501914

This PDF file includes:

- fig. S13. Loss of filamentation phenotype of Δ*crtS* mutants by the acquisition of compensatory mutations.
- fig. S14. MFA of crtS mutants before and after acquisition of compensatory mutations.
- fig. S15. The effect of MFA normalizations.
- table S1. Compensatory mutations obtained after evolution of Δ*crtS* mutants.
- table S2. List of plasmids and bacterial strains.
- table S3. Primers used in qPCR.
- Legends for movies S1 to S4
- References (*50–64*)

Other Supplementary Material for this manuscript includes the following:
(available at advances.sciencemag.org/cgi/content/full/2/4/e1501914/DC1)

- movie S1 (.avi format). 3D representations of the contact map from fig. S9 (exponential growth of the WT in LB).
- movie S2 (.avi format). 3D representations of the contact map from fig. S9 (exponential growth of the WT in MM).
- movie S3 (.avi format). Time-lapse fluorescence microscopy of Δ*crtS* filamentous cells, tagged at VC783 (Chr1) and near ori2 (Chr2), growing on an M9 MM agar pad supplemented with fructose and thiamine.
- movie S4 (.avi format). Time-lapse fluorescence microscopy of Δ*crtS* filamentous cells, tagged at VC783 (Chr1) and near ori2 (Chr2), growing on an M9 MM agar pad supplemented with fructose and thiamine.

SUPPLEMENTARY MATERIAL AND METHODS

Strain constructions

General procedures

Unless otherwise stated, bacteria were grown in LB lennox (rich medium) or M9 (minimal medium). Antibiotics were used at the following concentrations: carbenicillin, 100 µg/ml; chloramphenicol, 25 µg/ml for *Escherichia coli* and 5 µg/ml for *Vibrio cholerae*; kanamycin, 25 µg/ml; spectinomycin, 100 µg/ml; rifampicin, 1µg/ml; zeocin, 25 µg/ml. Diaminopimelic acid was used at 0.3 mM, X-Gal at 120µg/ml, thymidine (dT) at 10 µg/ml, glucose at 1%, fructose at 1% and arabinose at 0.2% (w/v). For cloning purposes in R6K *γ-ori*-based suicide vector, Π3813 was used as a plasmid host (*50*). For conjugal transfer of plasmids to *V. cholerae* strains, *E. coli* β3914 was used as the donor (*50*). Natural transformation was performed according to the procedure described in (*51*). Genomic DNA was extracted using DNeasy® Tissue Kit (Qiagen). Plasmid DNA was extracted using the GeneJET Plasmid Miniprep Kit (Thermo Scientific, Lafayette, CO, USA). PCR assays were performed using Phusion High-Fidelity PCR Master Mix (Thermo Scientific, Lafayette, CO, USA). DNA concentration was measured on a NanoDrop ND1100 (Thermo Scientific, Lafayette, CO, USA).

ESC2 and CSV2 construction

V. cholerae genome rearrangements were carried out following the procedure described in (*18*). Briefly, *attL/R* site-specific recombination sites from phages λ and HK022 are inserted on *V. cholerae* chromosomes by homologous recombination. In all cases, *attR* and *attL* sites were placed in intergenic zones of inversely oriented ORFs to avoid gene or operon interruption. PCR products carrying an *att* site, an antibiotic resistance cassette and two 500bp flanking homologous sequences were generated by two-step PCR. Following the procedure of (*51*), PCR products were then transformed by natural transformation into WT (N16961C*hapR*Δ*lacZ*). On Chr2, $attL_{HK}$ was inserted between VCA628/629 and $attR_{\lambda}$ was inserted between VCA514/515. In this strain, partner sites $attL_{\lambda}$ and $attR_{HK}$ were integrated at different locations on Chr1 to generate ESC2 and CSV2. For ESC2: $attL_{\lambda}$ was inserted between VC981/982 and $attR_{HK}$ was inserted between VC1939/1940. For CSV2: $attL_{\lambda}$ was inserted between VC1110/1111 and $attR_{HK}$ between VC1650/1651. A vector expressing [int_{λ}-xis_{λ}, int_{HK}-xis_{HK}] (pMP96) was conjugated into the strains containing all four *attR/L* sites to catalyze the recombination between the *att* sites which will produce rearrangements between Chr1 and Chr2. Selection of the mutants was carried out using reporter genes as already described in (*18*).

Inversion of large DNA fragments in Chr1

Following the procedure described in (*52*), *attL* and *attR* recombination sites derived from phage HK022 associated to either the 5' or the 3' portion of the β-lactamase gene (*bla*) were inserted in intergenic regions on the chromosomes of *V. cholerae*. Recombination events between $attR_{HK}$ and $attL_{HL}$ regenerate *bla*, conferring resistance to carbenicillin, allowing selection of these mutants on carbenicillin-containing selective medium (*52*). *attL* and *attR* sites were inserted in the opposite orientation to each other so that the *att*-flanked DNA fragment is inverted upon recombination. Recombination between an $attL_{HK}$ inserted between VC18/19 and $attR_{HK}$ inserted between VC392/393, VC590/591, VC659/660, VC771/772, VC963/964 gave rise to JB392, JB590, JB659, JB771 and JB963, respectively.

Deletion of *crtS*

Genome alteration was achieved through homologous recombination between the chromosomal region of interest and a PCR product generated by two-step PCR that contains the antibiotic-resistance cassette flanked by 500 bp sequences homologous to the target DNA. *V. cholerae* was naturally transformed with the PCR products as described in (*51*). To delete *crtS*, the 150 bp Chr1 sequence (coordinates 817950-818100) was replaced by a rifampicin-resistance gene (*arr2*). This sequence corresponds closely to the chrI-4 sequence (coordinates 817947-818099) that was replaced by a *FRT* site by Baek *et al.* (*12*). All mutants were verified by PCR and sequencing (using primers forward TGTGGTCGTTCATCGTCTTG and reverse TCGCCCATTCACTTGATCCG) and by PFGE for their genome structure. The 3 mutants that were studied in more detail (*crtS#7*, D185, D247) were subjected to whole genome sequencing (for MFA studies), allowing detection of genome rearrangements, gene amplifications and mutations. Genome comparison with their parental strains allowed us to follow the appearance of spontaneous mutations, duplication events

or genome rearrangements, which often occurred in the genetically unstable *crtS* mutants. Due to their instability, experiments were always started from the original sequenced -80°C stock.

Transposition of *crtS* to various locations on Chr1

We transposed a 170 bp sequence (coordinates 817931 – 818100), enclosing the chrI-4 fragment (*12*). We used our own collection of *V. cholerae* mutants in which site-specific recombination cassettes ([*bla'-attR*$_{HK}$]-*aph*-[*attL*$_{\lambda}$-*'lacZ*]) have been inserted at various positions along the two chromosomes, in chosen intergenic regions of inversely oriented ORFs to avoid gene or operon interruption. To transpose *crtS* to other genomic loci, we generated a conjugative R6K *γ-ori*-based suicide vector carrying a cassette containing *crtS* and the chloramphenicol acetyl transferase antibiotic marker flanked by *att* sites ([*lacZ'-attR*$_{\lambda}$]-*crtS-cat*-[*attL*$_{HK}$-*'bla*]). The suicide plasmid was then transferred by conjugation to recipient *V. cholerae* carrying a vector expressing [*int*$_{\lambda}$-*xis*$_{\lambda}$, *int*$_{HK}$-*xis*$_{HK}$] (pMP96). Since the suicide plasmid cannot replicate in *V. cholerae*, selection of the plasmid's drug resistance cassette (chloramphenicol) usually resulted in mutants in which the chromosomal cassette (kanamycin) had been exchanged with the plasmid cassette by site-specific recombination between the *attL* and *attR* sites.

Quantitative PCR (qPCR)

Genomic DNA (gDNA) was prepared with the DNeasy® Tissue Kit (Qiagen) from 1ml of exponentially growing cells (OD_{450} ~ 0,15). Each measurement was replicated at least four times. Primer pairs amplify a 150bp product near *ori1* (VC2775) or *ori2* (VCA0003) (table S3). PCR efficiencies (95%-100% for each primer pairs) were determined from a standard curve that was generated by a 5-log dilution series of gDNA extracted from non-replicating cultures in stationary phase. The standard curve provided a reference for relative quantification of exponentially growing samples. Relative loci abundances (*ori1*, *ori2*) were then used to generate ratios. Quantitative PCR was conducted on an ABI PRISM® 7900HT Sequence Detection System (Applied Biosystems) using the SYBR® green PCR master mix (Applied Biosystems), according to the manufacturer's instructions.

Marker Frequency Analysis (MFA)

Sequencing

Cells were grown in LB (+ glucose) at 30°C under agitation. Genomic DNA was prepared using the DNeasy® Tissue Kit (Qiagen) from 30ml of exponentially growing cells (OD_{450} ~0.15). The remaining culture was kept under agitation at 30°C to determine the generation time corresponding to each sample. gDNA samples were quantified using a Qubit Fluorometer (Life Technologies). Sequencing libraries were prepared for sequencing by automat, targeting an insert size of 200 bp. Libraries were sequenced using an Ion Proton sequencer (Life Technologies). PI chip was used to generate >5 million unique reads for each sample. These reads were on average greater than 100 bp long.

Analysis

MFA was performed essentially as described in (*17*). Reference sequences corrected for the *ori1* inversion (fig. S1) and the CSV2 and ESC2 genome rearrangements were constructed. Short reads were aligned to reference sequences using R2R and the number of reads starting per bp (N) were calculated for 1 kbp and 10 kbp windows. Any window including repeated sequence was excluded, and N was plotted as a function of position (the replichore of Chr1 = 2961 / 2 = 1480.5 kbp was set to one, origin centered and left and right side of *ter* set to -1 and 1 respectively for wt). This scale was kept for Chr2.

Each window was corrected in two steps. First, we normalized the reads of each window to the reads of the same window from an out-grown culture where replication is completed and each window therefore should have the same number of reads. Next we established a correction factor based on the average of the deviation of each 1 kbp window from the average of 40 windows in 4 samples. The effect of these corrections is shown in fig. S15.

ter1 & *ter2* were placed opposite to *ori1* & *ori2*; the location was visually verified; the marker frequency was taken as the average of 50 windows on each side of the *ori* or *ter*, and windows with repeated sequences were filtered out. The small bias in *ori* copy being too low and *ter* being too high was not compensated.

Interpretation

The marker frequency at various positions in a DNA fragment will vary when the replication time for a DNA fragment is significant compared to the generation time of the cells harboring this DNA fragment. For a circular chromosome the marker frequency will be highest at the origin and lowest at the terminus.

The frequency of a sequence, N_x, at any position m_x, for a homogenous steady-state culture with a constant replication speed is given by the formula (*53*)

$$\frac{N_x}{N_y} = 2^{(m_y - m_x)\frac{C}{\tau}} \quad (1)$$

where N_x and N_y are the frequencies of the relative positions, m_x and m_y, on a replichore, relative to *oriC* (m is 0 for *oriC*; -1 and 1 at the terminus for the left and the right replichore, respectively). τ is the doubling time for the culture, and C is the replication time for this replichore. For the position $m_y = 0$ (*oriC*), Equation 1 becomes (*17*)

$$N_x = N_{oriC} \times 2^{-\frac{m_x C}{\tau}} \quad (2)$$

where N_{oriC} is the frequency of *oriC*. A semi-logarithmic graph of the marker frequency of a sequence as a function of its distance to the origin will give a straight line and have the slope

$$\frac{\mathrm{d}(\log_2 N_x)}{\mathrm{d}m_x} = -\frac{C}{\tau} \quad (3)$$

A discontinuous graph will indicate chromosomal rearrangements in the sample compared to the reference sequence and deviations from the slope will indicate variations in the replication speed (*17*).

This graph will indicate the timing of replication at the various positions, m_x, relative to the initiation at *oriC*. For example, it follows from equation [2] that $N_x = 0.5 \times N_{oriC}$ for the relative position $m_x = \tau/C$; therefore, that position m_x is replicated one doubling time, τ, after initiation. This will time-wise coincide with the following initiation at *oriC* as a consequence of the overlapping cell cycles (*54*).

In this work we have superimposed the marker frequency graphs for Chr1 and Chr2 and scaled the graphs so one unit on the x-axis corresponds to one replichore of Chr1. Positions on the two chromosomes replicated simultaneously in the cell will have the same marker frequency. Further, the overlapping cell cycles imply that two positions with a two-fold difference in their copy-numbers will also be replicated simultaneously, but their replication is part of each of two successive cell cycles.

Short-Term Evolution Experiment

Cells were grown in Mueller Hinton medium (MH) at 37°C under agitation. Each culture of mutant strains was diluted in fresh medium every morning and every evening, allowing them to grow seven generations during the day and nine generations overnight. Details are given in the Supplementary Material. Based on the volume of media in the flasks (as Volume = 2^n, with n = # of generations of bacteria), and to minimize bottleneck effects, 1 ml of the previous culture is added to the fresh medium, with a 1:128 dilution factor for day growth and a 1:512 dilution factor for overnight growth. The extended time allowed for growth allows the slowest-growing mutant to reach stationary phase before proceeding to the next dilution. A 1ml sample was stored every morning at -80°C for further PFGE and MFA analysis.

Pulsed-Field Gel Electrophoresis (PFGE)

Strains were grown overnight in LB with agitation at 37°C. Cells were pelleted from 1ml of culture, washed in 10mM Tris-HCl (pH 8.0), 1M NaCl and 50mM EDTA, and mixed with an equal volume of molten low-melting-point 1.6% agarose (Chromosomal grade agarose, Bio-Rad). Agarose plugs were incubated for 2h at 37°C in lysozyme solution (1mg/ml lysozyme in 10mM Tris-HCl, (pH 8.0), 1M NaCl, 100mM EDTA, 0.2% sodium deoxycholate, 0.5% N-lauryl sarcosine sodium (SLS) and 2

µg/ml RNAase) and then in 1mg/ml proteinase K in 0.5M EDTA (pH 8.0) and 1% SLS at 50°C overnight. Cell debris and proteinase K were removed by four washes in 20mM Tris-HCl (pH 8.0) and 50mM EDTA for 2h each at room temperature. The native chromosomes were resolved by PFGE in a 0.8% agarose gel (Pulse Field certified agarose, Bio-Rad) in 0.5X TAE (40mM Tris-acetate, 1mM EDTA [pH 8.0]) at 14°C on a CHEF DR III System (BioRad). Electrophoresis conditions were, for block 1: 72h, initial pulse time of 20 min, final pulse time of 29 min 45 s, angle of 120°, at 2 V/cm; and for block 2: 32h, initial pulse time of 40.85 s, final pulse time of 2 min 25.98 s, angle of 120°, at 2 V/cm). Gels were subsequently stained with Ethidium Bromide and visualized on a Molecular Imager Gel Doc XR System (BioRad).

Fluorescence Microscopy

Cells were grown in LB at 37˚C until OD_{600} ~0.6, then 1:100 diluted in M9 media (10 µg/ml dT, 1% fructose) and grown at 37˚C until OD_{600} ~0.6, then 1:000 diluted in 5 ml M9 media (10 µg/ml dT, 1% fructose) and grown overnight at 25°C. The next day, the cultures were 1:4 diluted in M9 media (10 µg/ml dT, 1% fructose) and grown at 37˚C until a density of OD_{600} ~0.2. An agar pad (1% agarose in M9) was cast on a slide and 2µl of cell culture was adsorbed onto the pad before addition of a cover-slip. Cells were visualized using a Leica DM6000 B microscope. Analysis of snapshots was performed using the MATLAB-based software MicrobeTracker Suite (*55*). Data analysis was performed using MATLAB scripts described in (*19*). Timelapses were acquired as previously described (*19*) with a microscope Axio Observer (Zeiss) coupled with a CSU 1x Spinning Disk, a 491 laser illumination line and a EVOLVE 512 EM-CCD camera (Roper scientific).

Chromosome Conformation Capture (3C)

Construction of 3C libraries

Briefly, cells were grown in 100 ml of LB medium (10^6 cells/ml) at 30°C until a final concentration of ~1-2 x 10^7 cells/ml. Cells were then crosslinked using fresh formaldehyde for 30 minutes at room temperature (3% final concentration; Sigma Aldrich Formalin 37%) followed by 30 minutes at 4°C. Formaldehyde was quenched with a final concentration of 0.25 M glycine for 5 minutes at room temperature (RT) followed by 15 minutes at 4°C. Fixed cells were pooled in aliquots of 10^9 cells, collected by centrifugation, frozen in dry ice and stored at -80°C.

Frozen pellets of ~10^9 cells were thawed on ice and suspended in a final volume of 650 µl 1X TE (pH 8), and 4 µl of Ready Lyze lyzozyme (35 U/µl; tebu-bio) was added. Samples were then Samples were then processed as described (*23*).

Processing of libraries for Illumina sequencing

5 µg aliquots of each 3C library were dissolved in water (final volume 130 µL) and processed as described (*23*). For each library, several PCR reactions were performed to determine the optimal amount of template and number of cycles. Eight independent PCR reactions were then performed using the optimal protocol, whose products were purified on Qiagen MinElute columns and paired-end sequenced on an Illumina platform (HiSeq2000, HiSeq2500 or NextSeq).

Processing of PE reads

Sequencing data for each library was de-multiplexed using the corresponding tags present on the custom-made adapters and processed as follows: First, PCR amplification duplicates, identified as sharing identical hexanucleotide sequences at the 6Ns position present on each adapter, were discarded. Each read of a pair was then aligned independently using Bowtie 2 in its most sensitive mode (*56*). We used an iterative alignment procedure similar to (*57*), with a mapping quality above 40.

Generation of 3C contact maps

Each mapped read was assigned to a restriction fragment. Pairs of reads separated by less than 7 restriction sites were discarded from the analysis, since they correspond most likely to looping events of undigested DNA molecules, as described in (*58*). Because these restriction fragments present a large heterogeneity in sizes, we chose to bin the genomes into regular units (or bins) of 5 kb segments to generate contact maps.

Contact maps were then normalized using the sequential component normalization procedure (SCN) (*58*). The SCN procedure ensures that the sum over the column and lines of the matrix

equals 1, which compensates for the heterogeneity in the various restriction fragments and therefore reduces the biases inherent to the protocol. The 2% of bins showing the widest distribution (i.e. standard deviation) were set to 0.

Identification of domain borders using directional index

To quantify the degree of directional preference for a given bin, we applied on our correlation matrices a procedure very similar to the one used in (*23, 25*). More precisely, for each 5 kbp bin, we extracted the vector of interactions from the correlation matrix between that bin and bins at regular 5 kbp intervals, up to 100 kbp in both left and right directions. We then compared the two vectors with a paired t-test to assess whether the strength of interactions remain significantly stronger in one direction relative to the other. A value of 0.05 was used as a threshold to assess a statistical significant difference. The directional preferences for the bin along the chromosome are represented as a bar plot with positive and negative t-values shown as red and green bars, respectively. The bars of the bins with t values below -2 or above 2 (corresponding to a p-value = 0.05) were trimmed for clarity of presentation. Between two domains identified in the contact matrixes (CID), the directional preference of bins changed dramatically, as illustrated by alternating red and green colors.

Transcription signal

RNAseq data from (*59*) (accession no. GSE62084) were processed as follows: Raw reads were mapped on the *V. cholerae* genome using Bowtie 2. The genome was then split into bins of 5 kbp and the RNAseq signal was summed for each bin. The signal was then normalized using the smoothed coverage data obtained from 3C experiments. Only the 15% highest expressed bins were represented.

Circos plot

Circos plot was used to obtain a semi-circular representation of the interaction of *ori2* and *ter2* with Chr1 (*60*). Only the 50Kb surrounding *ori2* and the 100 Kb surrounding *ter2* were considered. Among those interactions, we selected the 25% strongest interactions, divided them into 7 classes (25%-20%, 20%-15%, 15%-10%, 10%-7.5%, 7.5%-5%, 5%-2.5%, 2.5%-1%, <1%) and colored them, respectively, in very light grey, light grey, grey, very light blue, light blue, dark blue, very dark blue and extremely dark blue.

Multi-scale domainograms

The values, D(p,s), of the domainogram, D, at genome position, p, and scale, s, were computed as follows from the normalized Hi-C matrix, M: First, we computed the Pearson correlation matrix C from M using the corrcoef matlab built-in function. D(p,s) was then computed from C

$$D(p,s) = \sum_{i=1}^{s} C\ (p+i, p-i)$$

where D was normalized so that the minimum and maximum values for each scale, s, were set to 0 and 1, respectively (*23*).

3D topological representations of V. cholerae chromosomes

The reconstruction of 3D structures from SCN normalized Hi-C matrix was performed using ShReC3D (*26*). 3D structures were then processed and visualized using PYMOL (The PyMOL Molecular Graphics System, Version 1.7.4 Schrödinger, LLC).

SUPPLEMENTARY FIGURES

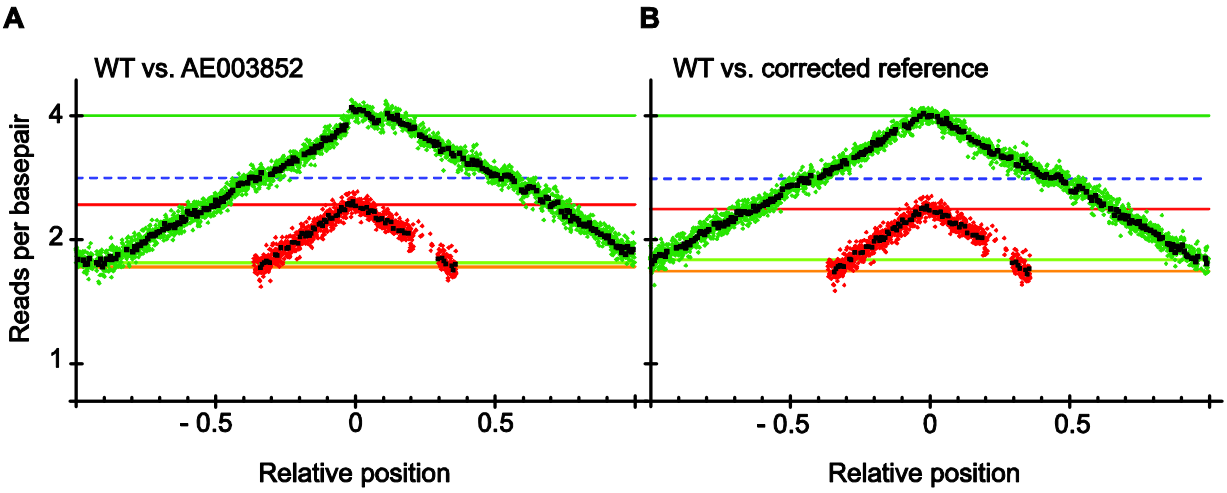

fig. S1. Chromosomal inversion detected around *ori1* when WT sequences are mapped against the National Center for Biotechnology (NCBI) reference genome AE003852. (**A**) The MFA plot of WT strain compared to the reference genome sequence (AE003852) indicated an inversion around *ori1* flanked by two ribosomal RNA operons (*rrnB and rrnG-H).* We found that our isolate of *V. cholerae* shared the same *rrnB - rrnG-H* orientation as other *V. cholerae* biotypes (*61, 62*) and other N16961 lab isolates provided by our collaborators (data not shown) suggesting that the observed inversion may have occurred in the isolate sequenced by (*6*). (**B**) MFA of WT against a corrected reference sequence of Chr1. Inversion of the DNA fragment between *rrnB* and *rrnG-H* on the N16961 reference sequence corrected the deviation.

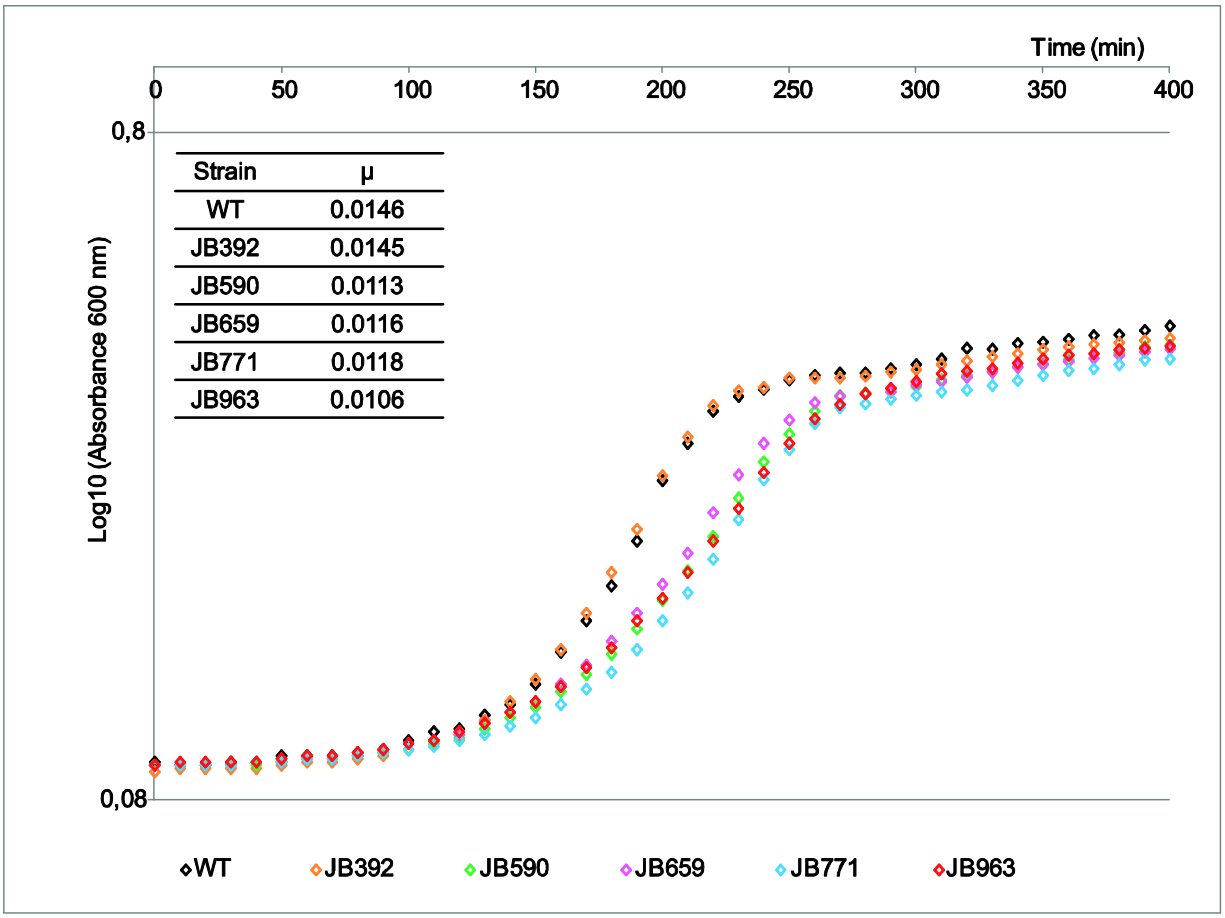

fig. S2. Large DNA inversions either caused no fitness cost (JB392) or were similarly affected (JB590, JB659, JB771, JB963). Growth curve comparison of WT, JB392, JB590, JB659, JB771 and JB963 using the Synergy 2 plate reader from BioTek. Overnight bacterial cultures were diluted 1/1000 in 1ml of LB medium. Cells were grown in a 24-well plate with medium shaking at 37°C. The plate was read every 10 minutes at 600nm. μ is the slope of the growth curve during exponential phase (min^{-1}).

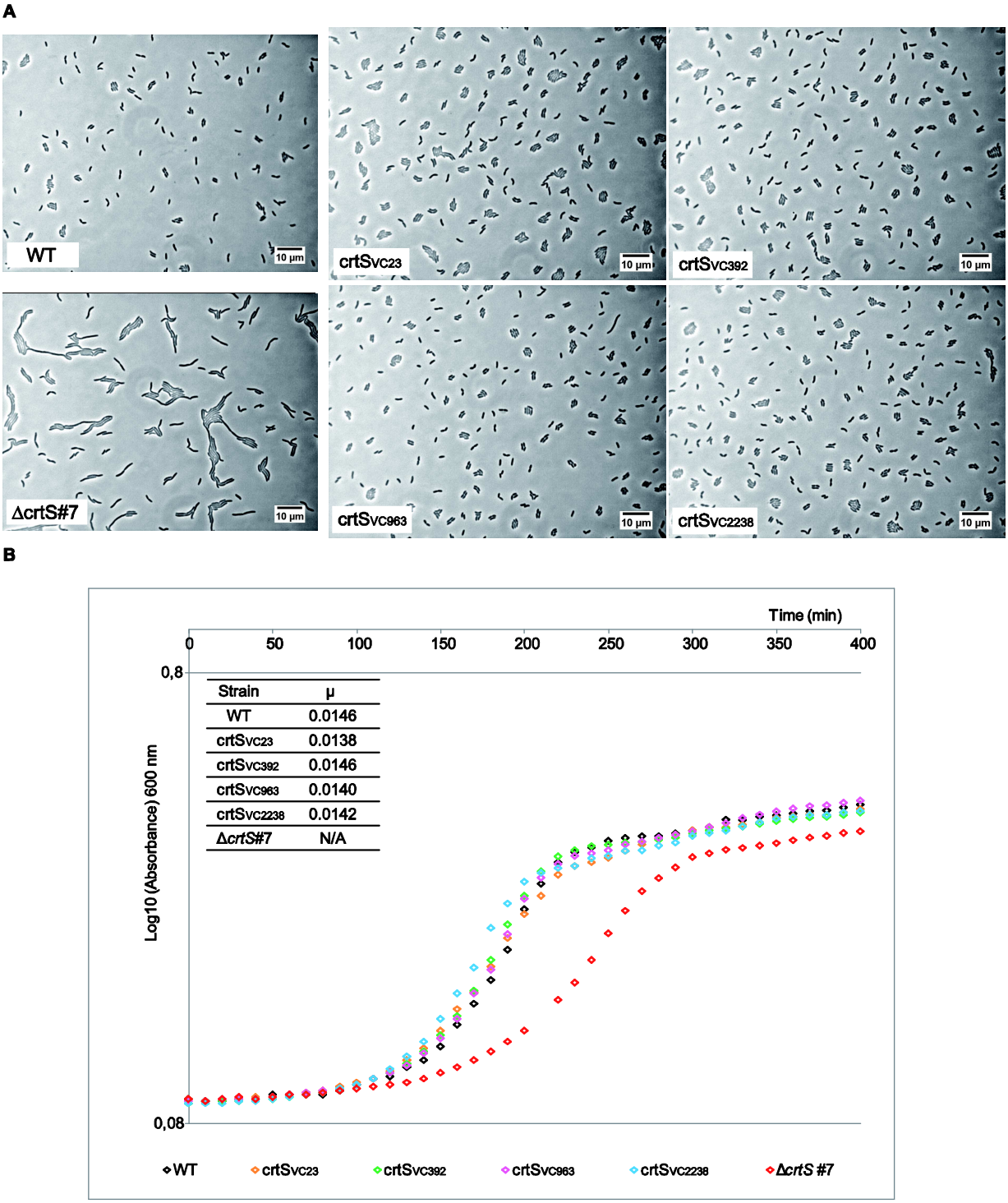

fig. S3. Complementation of Δ*crtS* filamentous phenotype by addition of an ectopic chromosomal copy of *crtS*. (**A**) Representative picture of *crtS*-relocated mutants observed by phase-contrast microscopy ($crtS_{VC23}$, $crtS_{VC392}$, $crtS_{VC963}$, $crtS_{VC2238}$) in comparison with WT and ΔcrtS#7 mutants. All *crtS*-relocated mutants display a WT phenotype. (**B**) Fitness recovery of Δ*crtS* mutants when *crtS* is re-inserted at ectopic sites on Chr1. Growth curve comparison of WT, Δ*crtS*#7 and *crtS* relocated mutants ($crtS_{VC23}$, $crtS_{VC392}$, $crtS_{VC963}$, $crtS_{VC2238}$) using the Synergy 2 plate reader from BioTek. Overnight bacterial cultures were diluted 1/1000 in 1ml of LB medium. Cells were grown in a 24-well plate with medium shaking at 37°C. The plate was read every 10 minutes at 600 nm. µ is the slope of the growth curve during exponential phase (min^{-1}). N/A (not applicable) because of the heterogeneous cell size population (cell filaments) in *crtS*-deleted mutants.

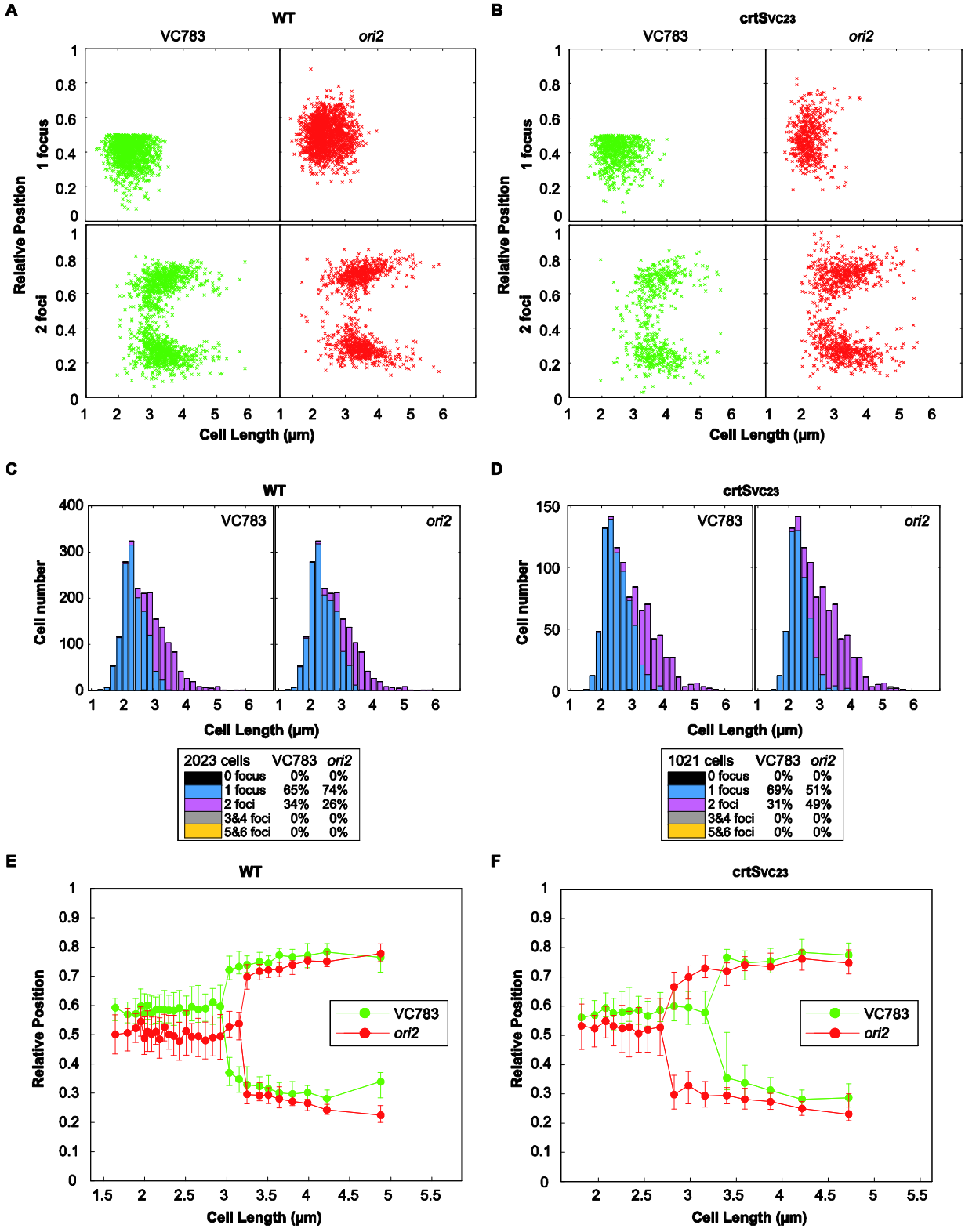

fig. S4. Duplication and segregation of VC783 and *ori2* foci in WT and mutant crtS$_{VC23}$ throughout the cell cycle. (**A-B**) Plot showing the position of VC783 (left panel) and *ori2* (right panel) foci inside WT (**A**) and mutant crtS$_{VC23}$ (**B**) cells. Foci are oriented longitudinally relative to the old pole of the cell as a function of cell length. The old pole of the cells was defined as the closest pole to a VC783 focus (this orientation is arbitrary as this locus is not strictly polarized toward the old pole). The x-axis represents cell length (µm). The y-axis represents the relative position of the focus in bacterial cells, 0 being the old pole and 1 the new pole. Snapshot images of 2023 WT and 1021 crtS$_{VC23}$ mutant cells were analyzed. (**C-D**) Histograms displaying the amount of cells that exhibit zero, one, two, three, four and five or six fluorescent foci according to cell size (µm) in WT

(**C**) and mutant $crtS_{VC23}$ (**D**) bacterial cells. (**E-F**) By correlating the longitudinal position of VC783 and *ori2* foci as a function of cell length, the segregation choreographies of the VC783 and *ori2* were reconstituted throughout the cell cycle of WT (**E**) and mutant $crtS_{VC23}$ (**F**) bacterial cells. Cells were classified according to their size and grouped by 30 to define each size interval. For most loci and cell length intervals, there were cells with either a single focus or two separated foci, the relative proportions of each type varying as a function of cell length. Only the position of foci corresponding to the dominant cell type in each cell length interval was plotted. The median positions of the observed foci (filled circles), along with the 25th–75th percentiles (error bars) were plotted for each cell size bin. The x-axis represents the cell length (µm). The y-axis represents the relative position of the focus in bacterial cells (0: new pole; 1: old pole).

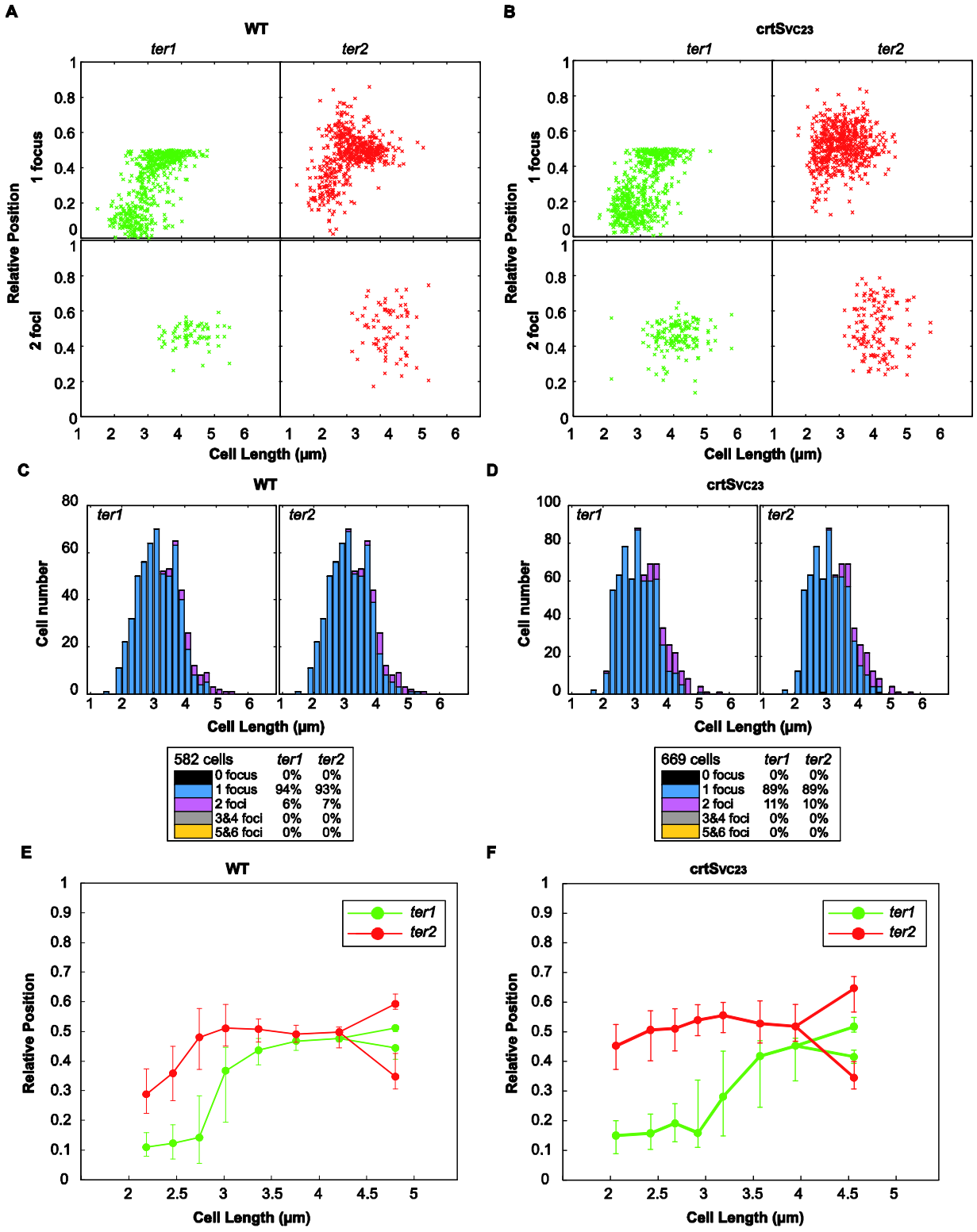

fig. S5. Duplication and segregation of *ter1* and *ter2* foci in WT and mutant crtS$_{VC23}$ throughout the cell cycle. (**A-B**) Plot showing the position of *ter1* (left panel) and *ter2* (right panel) foci inside WT (**A**) and mutant crtS$_{VC23}$ (**B**) cells. Foci are oriented longitudinally relative to the new pole of the cell as a function of cell length. The new pole of the cells was defined as the closest pole to a *ter1* focus. The x-axis represents the cell length (µm). The y-axis represents the relative position of the focus in bacterial cells, 0 being the new pole and 1 the old pole. Snapshot images of 582 WT and 669 crtS$_{VC23}$ mutant cells were analyzed. (**C-D**) Histograms displaying the amount of cells that exhibit zero, one, two, three, four and five or six fluorescent foci according to cell size (µm) in WT (**C**) and mutant crtS$_{VC23}$ (**D**) bacterial cells. (**E-F**) By correlating the longitudinal position

of *ter1* and *ter2* foci as a function of cell length, the segregation choreographies of the *ter1* and *ter2* were reconstituted throughout the cell cycle of WT (**E**) and mutant $crtS_{VC23}$ (**F**) bacterial cells. Cells were classified according to their size and grouped by 30 to define each size interval. For most loci and cell length intervals, there were cells with either a single focus or two separated foci, the relative proportions of each type varying as a function of cell length. Only the position of foci that correspond to the dominant cell type in each cell length interval was plotted. The median positions of the observed foci (filled circles), along with the 25th–75th percentiles (error bars) were plotted for each cell size bin. The x-axis represents the cell length (µm). The y-axis represents the relative position of the focus in bacterial cells (0: new pole; 1: old pole).

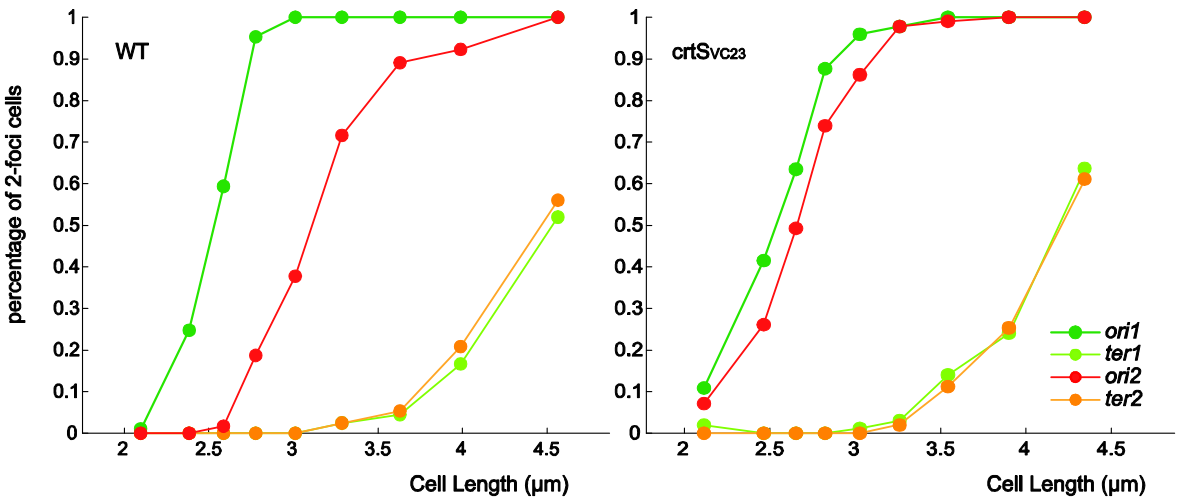

fig. S6. *ori2* foci duplicate earlier when *crtS* is located near *ori1*. Average percentage of two-foci cells in WT (left) and $crtS_{VC23}$ (right). Bacteria were grown in M9 minimal medium supplemented with fructose and thiamine. Loci were visualized in pairwise combinations: *ori1* - *ori2* and *ter1* - *ter2*. A total of 585, 2072, 582 and 669 cells were analyzed for WT (*ori1* - *ori2*), $crtS_{VC23}$ (*ori1* - *ori2*), WT (*ter1* - *ter2*) and $crtS_{VC23}$ (*ter1* - *ter2*) respectively.

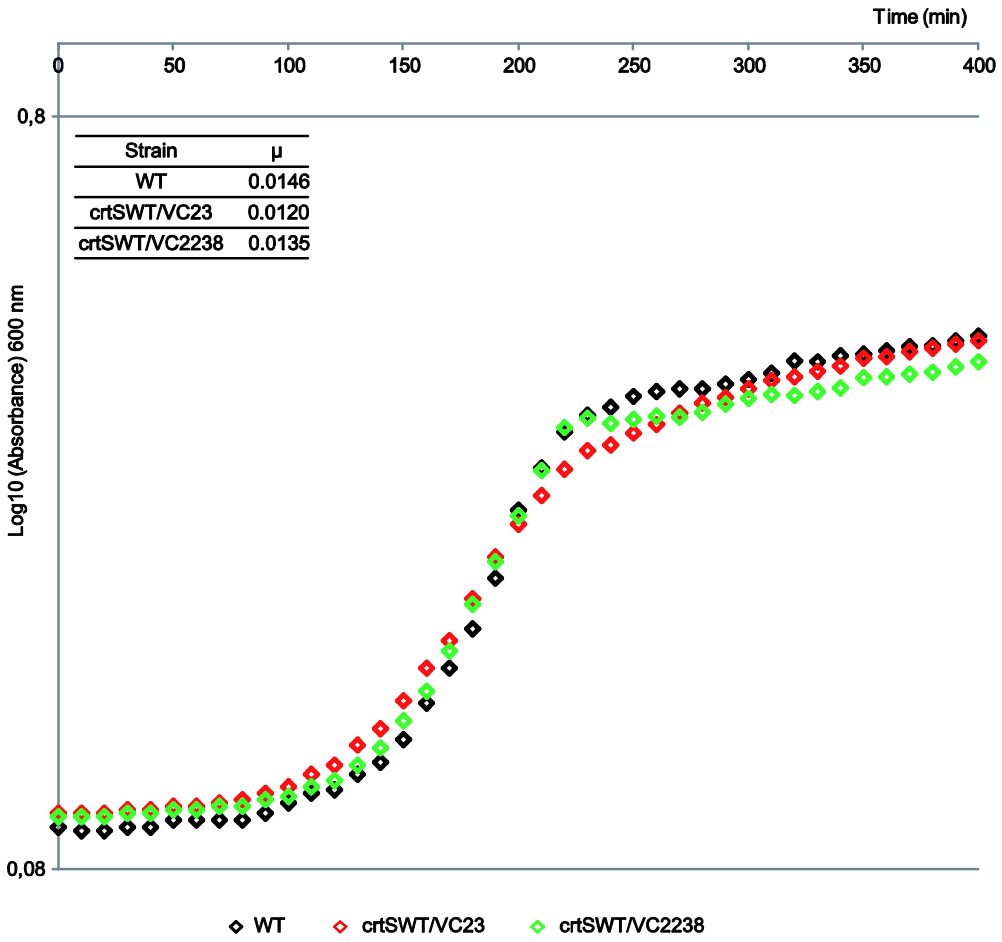

fig. S7. The addition of an extra copy of *crtS* affects the growth of *V. cholerae*. Growth-curve comparison of WT, $crtS_{WT/VC23}$ and $crtS_{WT/VC2238}$ using the Synergy 2 plate reader from BioTek. Overnight bacterial cultures were diluted 1/1000 in 1 ml of LB medium. Cells were grown in a 24-well plate with medium shaking at 37°C. The plate was read every 10 minutes at 600 nm. μ is the slope of the growth curve during exponential phase (min^{-1}).

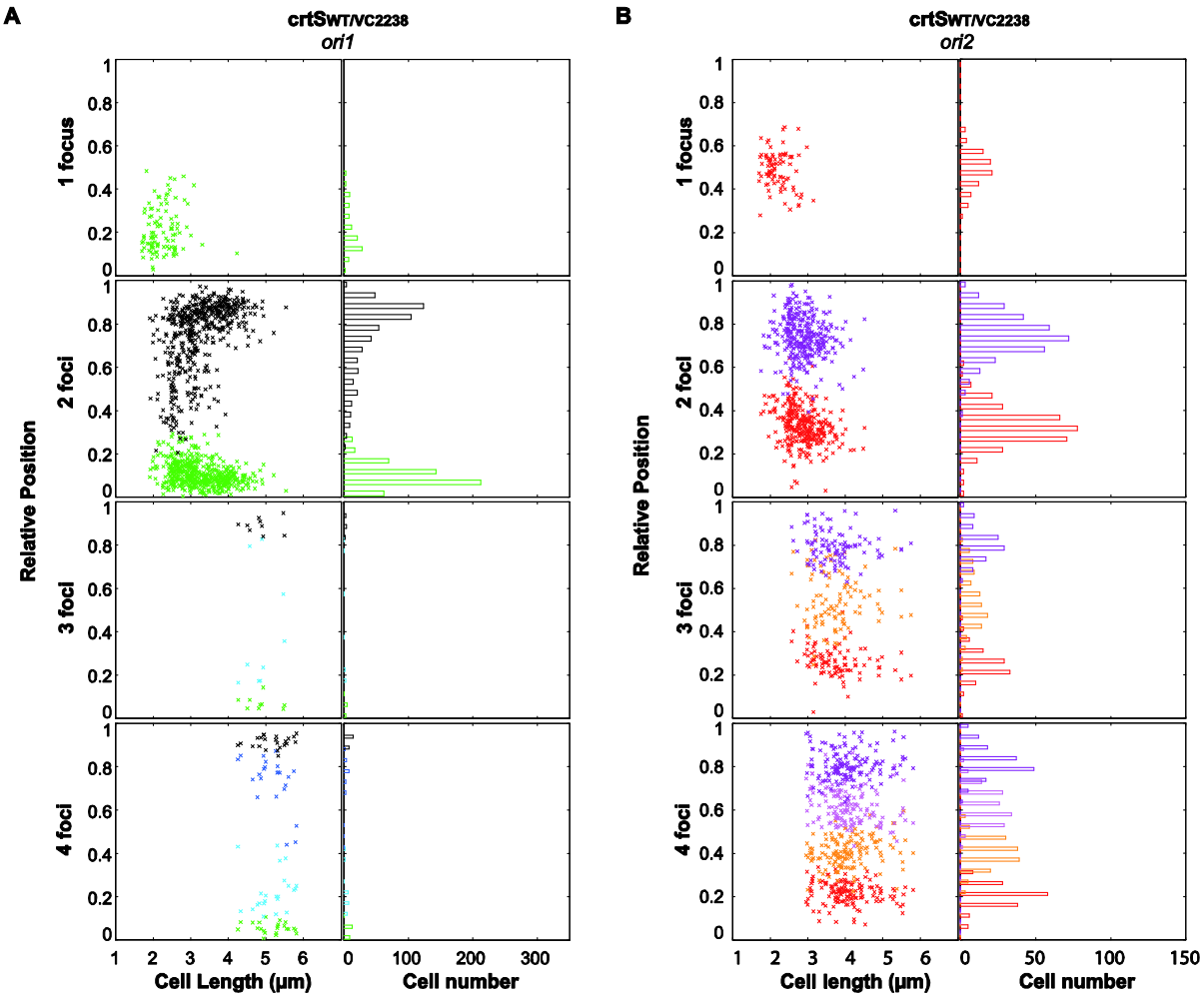

fig. S8. Doubling in *ori2* copy number in mutant with two chromosomal copies of *crtS*. (**A-B**) Position of *ori1* (**A**) and *ori2* (**B**) foci inside $crtS_{WT}/_{VC2238}$ cells. Foci are oriented relative to the old pole of the cell as a function of cell length. The old pole of the cells was defined as the closest pole to a *ori1* focus. On the left panel, the x-axis represents cell length (µm). On the right panel, the x-axis represents cell number. The y-axis represents the relative position of the focus in bacterial cells, 0 being the old pole and 1 the new pole. Snapshot images of 651 $crtS_{WT}/_{VC2238}$ mutant cells were analyzed.

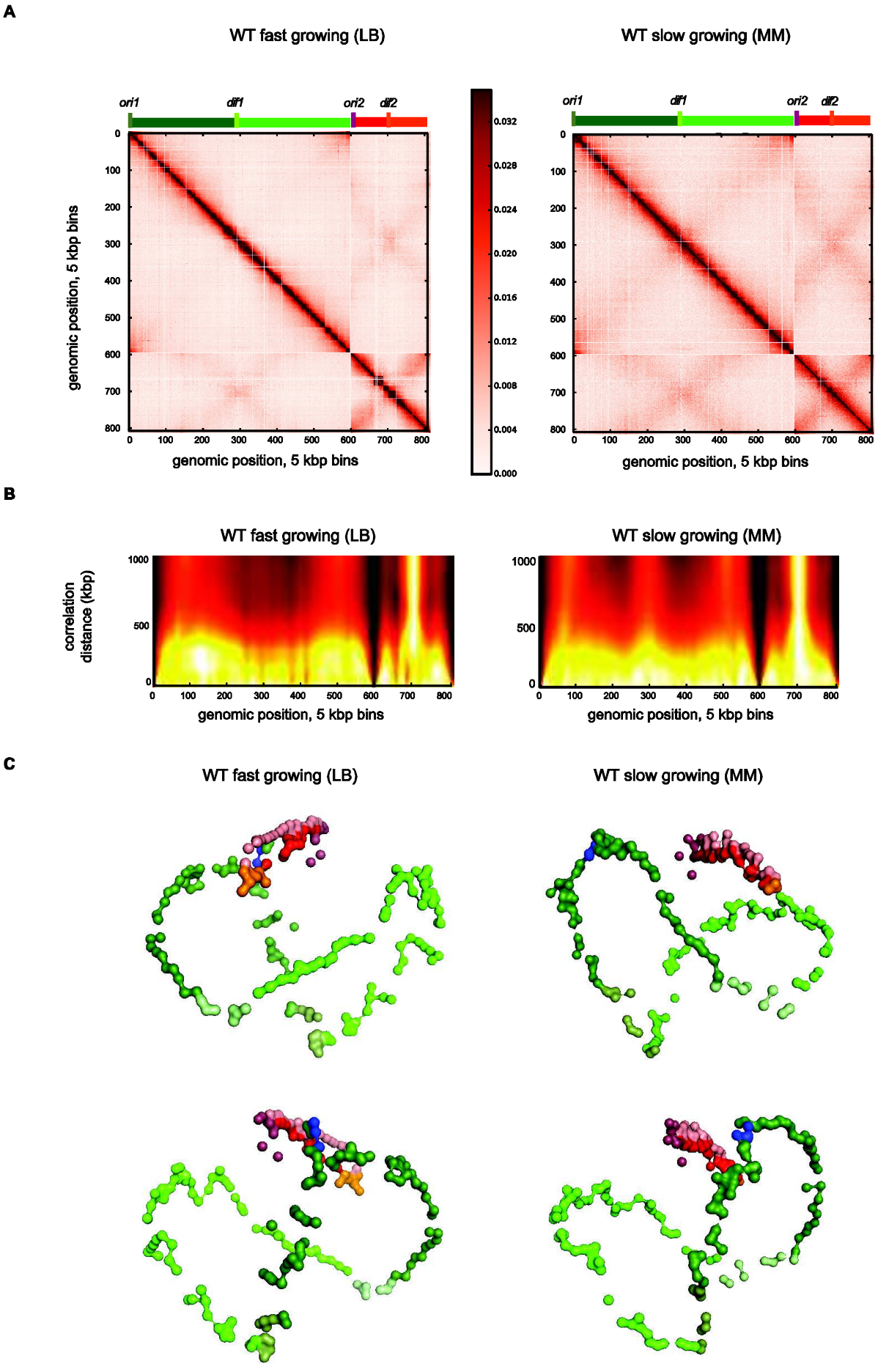
A
WT fast growing (LB)
WT slow growing (MM)
ori1
dif1
ori2
dif2
genomic position, 5 kbp bins
B
WT fast growing (LB)
WT slow growing (MM)
correlation distance (kbp)
genomic position, 5 kbp bins
C
WT fast growing (LB)
WT slow growing (MM)

fig. S9. Comparison of global chromosome organization of *V. cholerae* in different growth conditions. (**A**) Normalized and filtrated genomic contact map from asynchronous population grown in LB (left) or MM (right). Libraries were constructed using HpaII restriction enzyme. The same overall features could be observed for rapid (LB) and slow (MM) growing cells despite the presence of a weak secondary diagonal on Chr1 contact matrix for MM, which may reflect a difference in replication rate between the two conditions. Color code is the same as for Fig. 5. Noticeably, a strong secondary diagonal (perpendicular to the main one) reflecting inter-replichores contacts is only apparent on the Chr2 contact map. (**B**) Multiscale domainogram analysis of the matrices represented in (A). The two-dimensional pattern reflects the organization of the chromosome at multiple scales and allows detection of large domains (*23*). The x-axis represent the genomic coordinates while y-axis represents the length scale of the analysis. The signal of the secondary diagonal uniquely present in Chr2 is clearly visible in these representations. A difference in Chr1 folding in the two conditions is also visible. (**C**) 3D representation of the contact map from panel (A). Chromosomes are represented as a chain of beads (1 bead = 20 kbp). The beads' color-code is the same as in panel (A). *crtS* is represented in blue. Global overview of Chr1 and Chr2 topologies, achieved by converting it into a 3D representation (*26*).

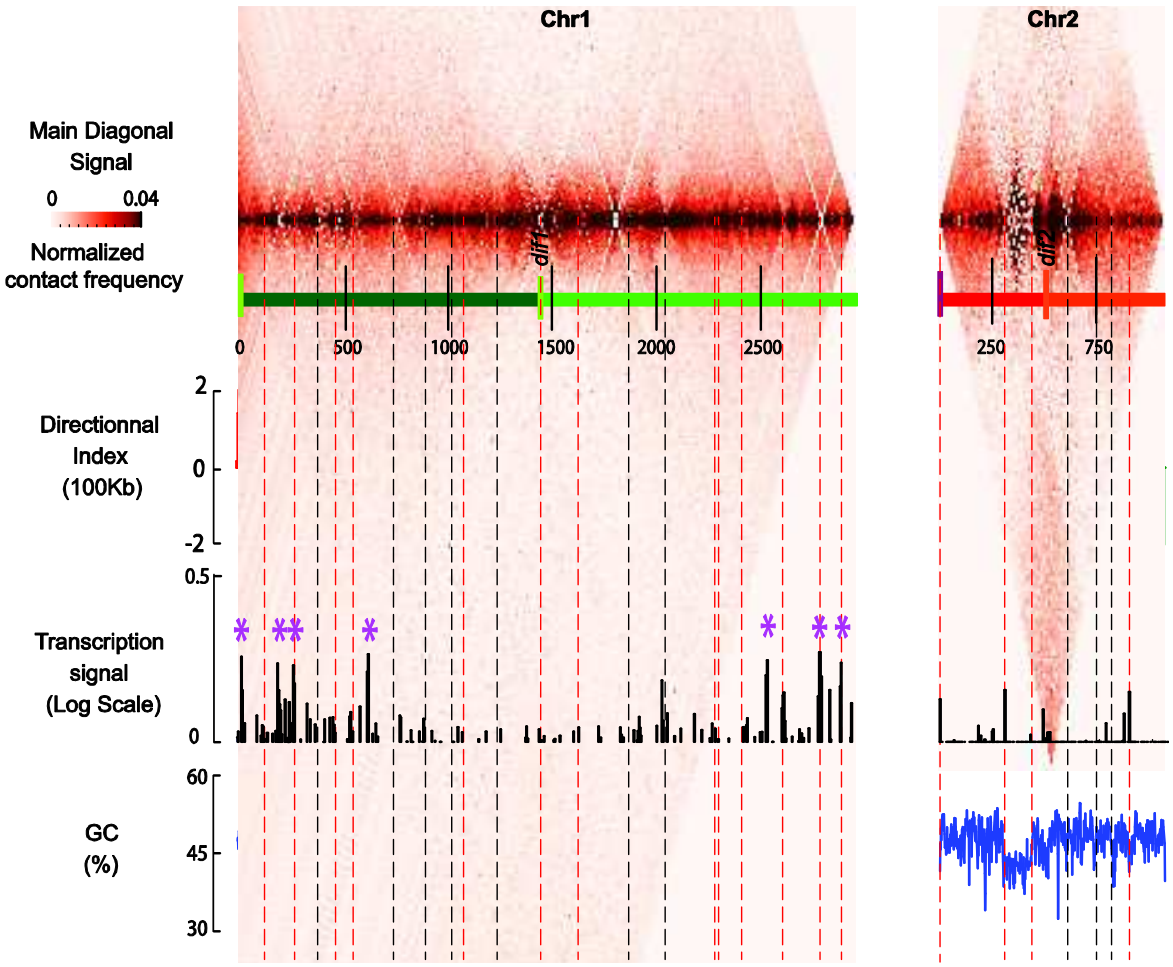

fig. S10. Comparison of directional index analysis at 100-kbp scale with transcription and GC content for fast-growing cells. From top to bottom: i) Magnification of main diagonal contacts of the *V. cholerae* genome for population growing in LB. ii) Scheme of *V. cholerae* genome. iii) DI analysis at 100 kbp scale. iv) Transcription signal (log scale; 5 kbp bins) (data from (*59*)), only the 15% most highly expressed bins are reported. v) GC content of *V. cholerae* genome with 5 kbp windows. Borders are represented as dashed lines. Red dashed line represents borders that correlate with transcription hotspots. Pink asterisks represent rDNA clusters. Examination of the main diagonal reveals squares of various sizes for the two chromosomes as previously described in other bacteria (*23, 25*). To decipher these small topological domains (CIDs), we performed an analysis using a directional index approach (DOI) (*63*) that reveals the presence of “barrier” regions in which contacts are low and the presence of subdomains between these barriers. At a scale of 100 kbp, we observed 27 statistically significant barriers and corresponding CIDs ranging from 20 kbp to 235 kbp (mean size = 150 kbp, Chr1 = 20 CIDs, Chr2 = 7 CIDs). These results are concordant with those previously obtained (*23, 25*). 60% (17/27) of the borders detected correlate with the presence of a highly expressed bin. This result suggests again that transcription is implicated in the establishment of CIDs. However, as previously observed (*23*), not all highly transcribed genes create a border, and some of the borders also correlate with GC content shifts (6 occurrences). Moreover, for rDNA clusters, which are part of the most transcribed bins, some do not create frontiers. Taken together, these observations suggest that the formation of CIDs is a highly dynamic process resulting from several factors, including transcription activity. The superintegron, a large gene capture and excision system located on Chr2 (*28*), defines a clear CID surrounded by two highly transcribed genes but also a strong GC shift.

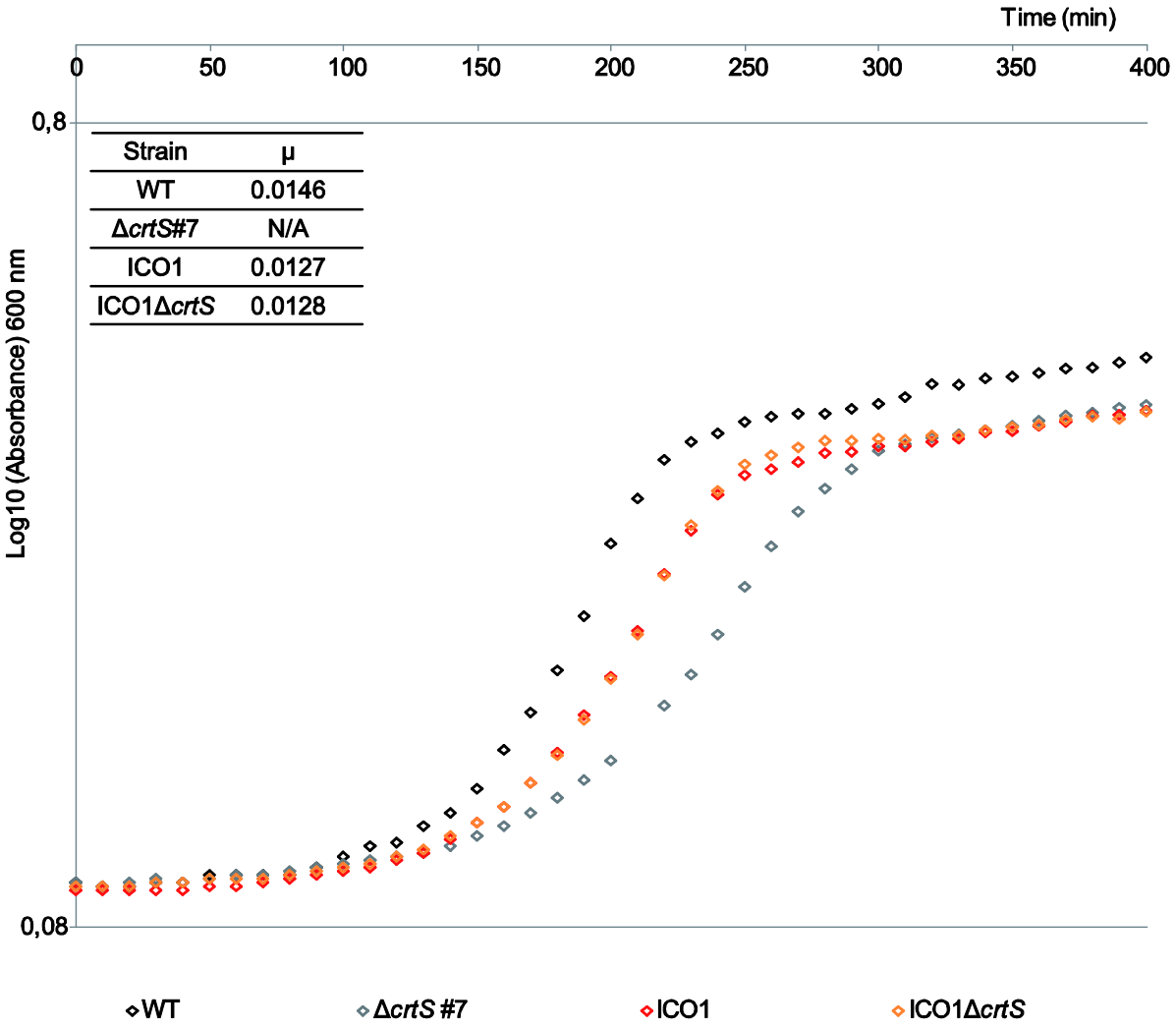

fig. S11. Δ*crtS* mutants have a fitness defect, whereas ICO1Δ*crtS* shows no additional growth defect. Growth curve comparison of WT, Δ*crtS*#7, ICO1, ICO1Δ*crtS* using the Synergy 2 plate reader from BioTek. Overnight bacterial cultures were diluted 1/1000 in 1 ml of LB medium. Cells were grown in a 24-well plate with medium shaking at 37°C. The plate was read every 10 minutes at 600 nm. μ is the slope of the growth curve during exponential phase (min^{-1}). N/A (not applicable) because of the heterogeneous cell size population (cell filaments) in *crtS*-deleted mutants.

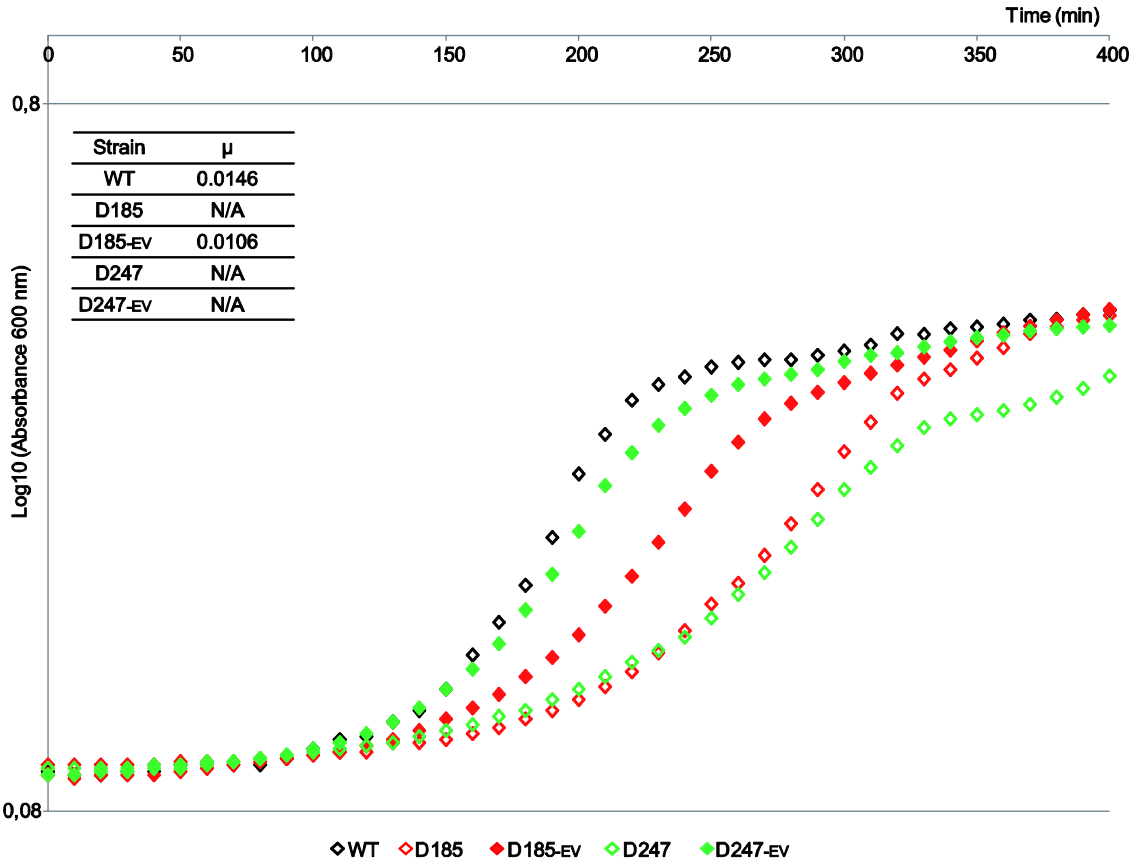

fig. S12. Fitness improvement of Δ*crtS* mutants by the acquisition of compensatory mutations. Growth curve comparison of WT, D185 and D247 before and after 200 generations ($_{-EV}$) using the Synergy 2 plate reader from BioTek. Overnight bacterial cultures were diluted 1/1000 in 1ml of LB medium. Cells were grown in a 24-well plate with medium shaking at 37°C. The plate was read every 10 minutes at 600 nm. μ is the slope of the growth curve during exponential phase (min^{-1}). N/A (not applicable) because of the heterogeneous cell size population (cell filaments) in *crtS*-deleted mutants.

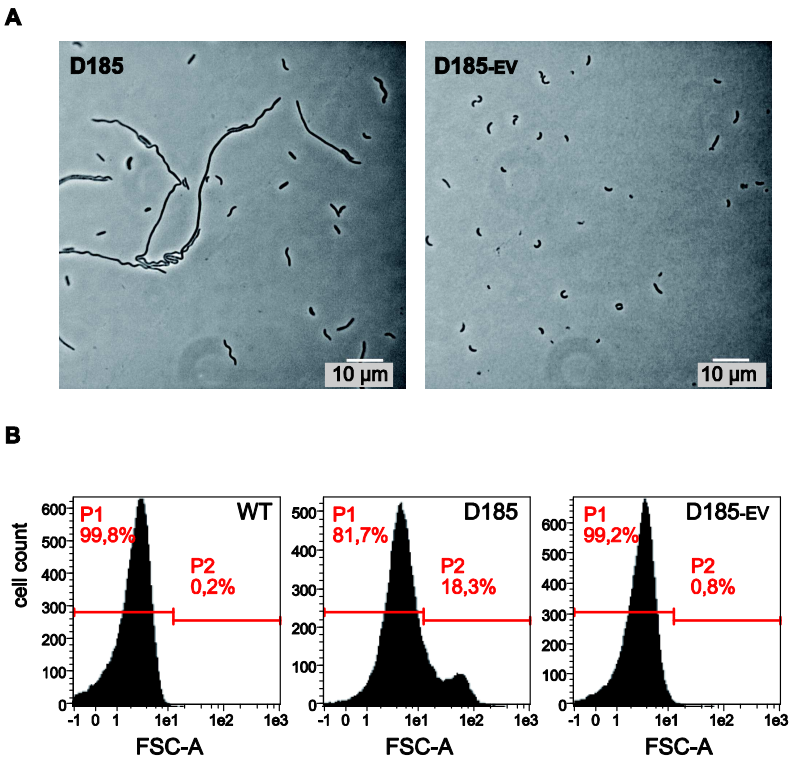

fig. S13. Loss of filamentation phenotype of Δ*crtS* mutants by the acquisition of compensatory mutations. (**A**) Representative picture of D185 and D185$_{-EV}$ observed by phase-contrast microscopy. (**B**) Cell size distribution of WT, D185 and D185$_{-EV}$ was determined by flow cytometry of cells grown in M9 (fructose, thiamine) using the MACSQUANT Analyzer (Miltenyi Biotec). The x-axis and y-axis represent Forward Scatter Area and cell count respectively. The proportion of normal size cells (P1) was calibrated on a WT population. P2 represents the proportion of abnormally longer cells. P1 and P2 regions are indicated by red lines.

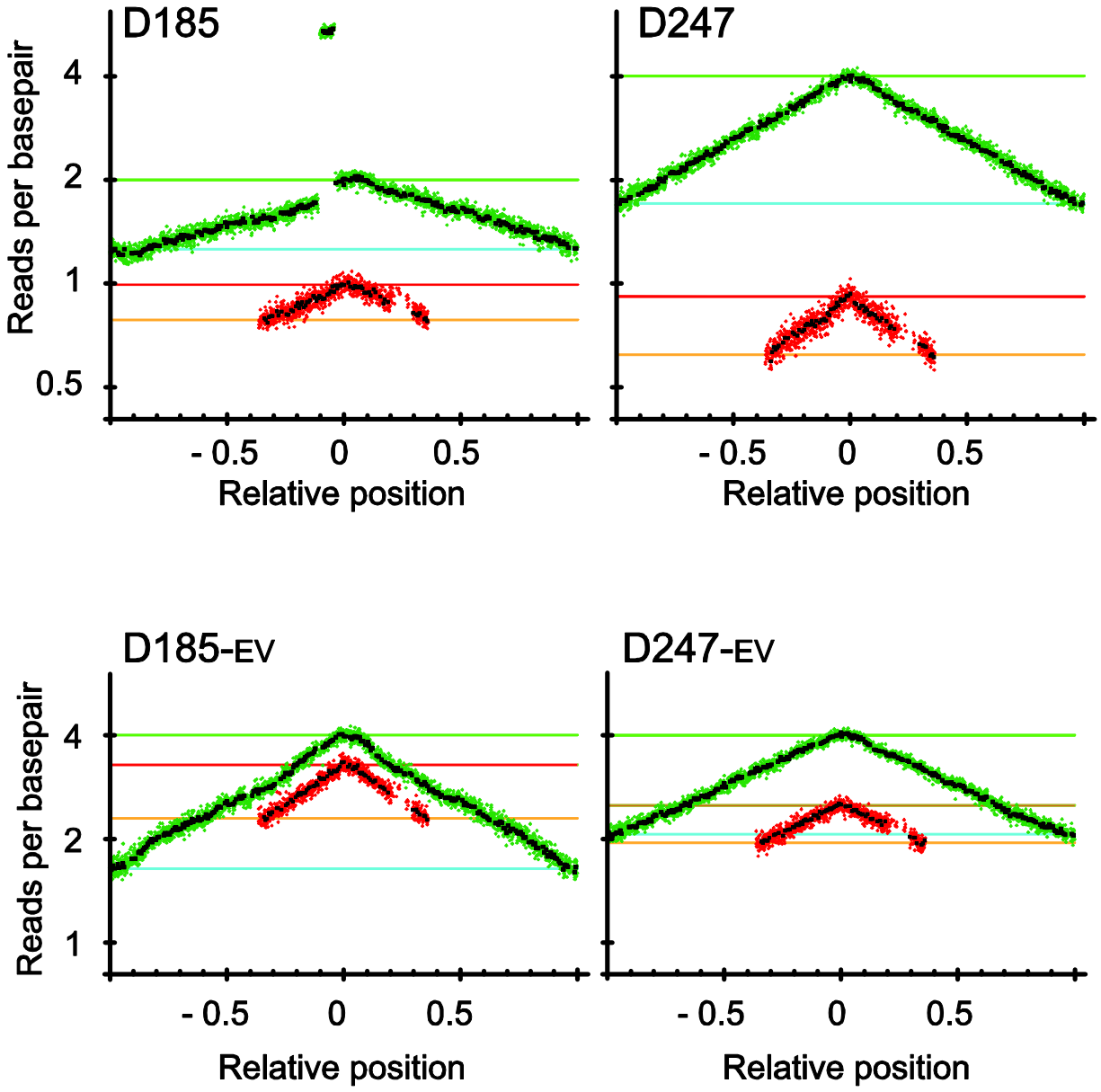

fig. S14. MFA of *crtS* mutants before and after acquisition of compensatory mutations. (**Top**) MFA of WTΔ*crtS* (D185, D247) before short-term experimental evolution. (**Bottom**) MFA of WTΔ*crtS* (D185-$_{EV}$, D247-$_{EV}$) evolved for 200 generations. MFA of D185 shows a 2.91-fold increased marker frequency for a region located between two ribosomal operons suggesting that this region has been triplicated. Chr2 in D185 is reduced in marker frequency; this can be explained by the mixed population apparent in fig. S13. D185-$_{EV}$ has restored the copy number of Chr2 to above WT-level and no longer shows the triplication near *ori1*. These duplication events between large homologous regions observed by MFA are not rare and could highlight a transient response to stress. MFA of D247 shows a reduced copy number of Chr2 but no other deviations from WT. D247-$_{EV}$ has restored the copy number of Chr2 to WT level, however the microscopy results indicate that this may just be the average of a mixed population containing one fraction with increased copy number and another fraction of filamentous cells with a lowered copy number.

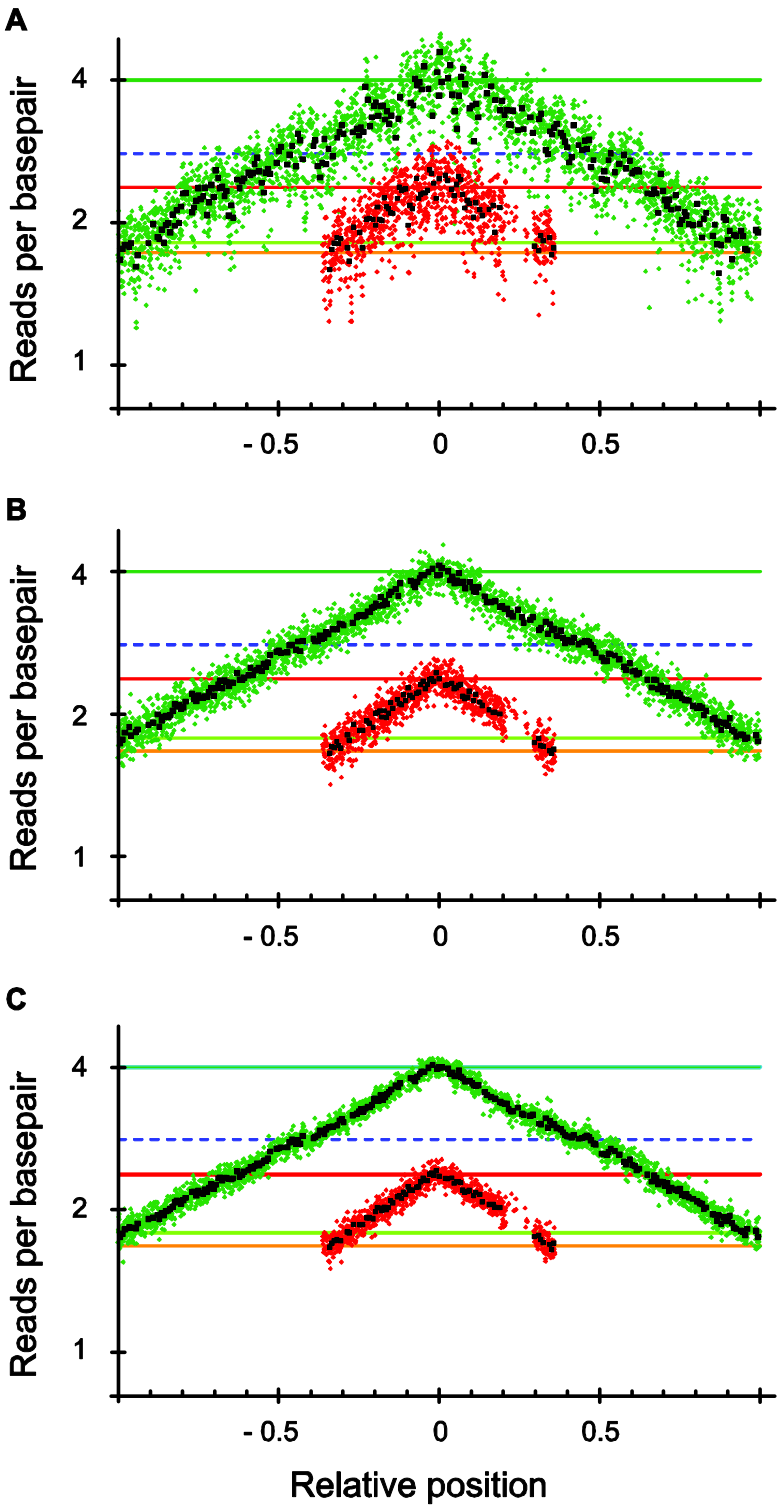

fig. S15. The effect of MFA normalizations. (A), Sequence reads were mapped, binned into 1 kbp and 10 kbp windows respectively, and the numbers plotted as a function of the positions on the chromosomes. Color codes and bars are as in Fig. 1. **(B),** The number of reads within each bin was normalized with the number of reads of that bin from an overnight culture where all replication forks had finished. **(C),** the number of reads within each bin was further corrected by a correction factor $\overline{C}_n$ based on 4 or more other datasets normalized as in (B). From each of these data sets a correction factor, C_n, was calculated for each bin, n, as: C_n = Mean[N_{n-20} .. N_{n+20}] / N_n; N_n is the number of reads in bin n. C_n was set to 1 for any bin with repeated sequence. Each bin from the data in (B) was then multiplied with the average of C_n, $\overline{C}_n$.

SUPPLEMENTARY TABLES

table S1. Compensatory mutations obtained after evolution of Δ*crtS* mutants.

Strain name *	Locus with the compensatory mutations	Compensatory mutations**
D247	29-mer (*rctB* promoter region)	TTGGAACTATAGTGATATTA(C/A)GGTAAGTG
D185	*rctB*	RctB (F230S)
C667	*rctB*	RctB (L357I)
C926	*rctB*	RctB (R195C)

* All strains have the same initial genotype (Δ*crtS*)
** present in the evolved strain (EV) and absent in the parental strain

table S2. List of plasmids and bacterial strains.

Name	Relevant genotype or features	Reference
Plasmids		
pMP7	Suicide plasmid for allele exchange - $oriV_{R6K\gamma}$ $oriT_{RP4}$ *araC*-P_{BAD}-*ccdB*	(*18*)
pHK-*crtS*	*crtS* transposition vector	This study
pMP96	pSC101*rep*(Ts) $oriT_{RP4}$ [int_{λ}-xis_{λ}, int_{HK}-xis_{HK}]	(*18*)
pAD19	*ori* R6K ; *lacZ*:: (YGFP-ParBT1, LacI-mcherry, *zeo*)	(*19*)
E. coli		
Π3813	B462 Δ*thyA*::(*erm-pir116*)	(*50*)
β3914	β2163 *gyrA462 zei-298*::*Tn10*	(*50*)
V. cholerae		
N16961	*Vibrio cholerae* serotype O1 biotype El Tor strain N16961	(*6*)
N16961*ChapR*	N16961::mTn*7hapR*	(*64*)
WT	N16961C*hapR*Δ*lacZ*	(*18*)
ESC2	Chr1and Chr2 rearrangement in WT, Chr1 = 2Mbp, Chr1 = 2 Mbp	This study
CSV2	Chr1and Chr2 rearrangement in WT, Chr1 = 2.5Mbp, Chr1 = 1.5 Mbp	This study
ICO1	*ori2* substitution with *ori1* on Chr2 in N16961	(*18*)
MCH1	Synthetic fusion of Chr1 and Chr2 in *V. cholerae* N16961	(*18*)
JB392	Chr1 inversion between intergenic regions VC0018/VC0019 and VC0392/VC0393	This study
JB590	Chr1 inversion between intergenic regions VC0018/VC0019 and VC0590/VC0591	This study
JB659	Chr1 inversion between intergenic regions VC0018/VC0019 and VC0659/VC0660	This study
JB771	Chr1 inversion between intergenic regions VC0018/VC0019 and VC0771/VC0772	This study
JB963	Chr1 inversion between intergenic regions VC0018/VC0019 and VC0963/VC0964	This study
WTΔ*crtS#1*	WTΔ*crtS::arr2* (strain #C667)	This study
WTΔ*crtS#2*	WTΔ*crtS::arr2* (strain #C919)	This study
WTΔ*crtS#3*	WTΔ*crtS::arr2* (strain #C925)	This study
WTΔ*crtS#4*	WTΔ*crtS::arr2* (strain #C926)	This study
WTΔ*crtS#5*	WTΔ*crtS::arr2* (strain #C927)	This study
WTΔ*crtS#6*	WTΔ*crtS::arr2* (strain #C928)	This study
WTΔ*crtS#7*	WTΔ*crtS::arr2* (strain #D137)	This study
ICO1Δ*crtS*	ICO1Δ*crtS::arr2*	This study
$crtS_{VC23}$	WTΔ*crtS with crtS* inserted between VC0023/VC0024	This study
$crtS_{VC392}$	WTΔ*crtS with crtS* inserted between VC0392/VC0393	This study
$crtS_{VC963}$	WTΔ*crtS with crtS* inserted between VC0963/VC0964	This study
$crtS_{VC2238}$	WTΔ*crtS with crtS* inserted between VC2237/VC2238	This study
$crtS_{WT/VC23}$	WT *with crtS* inserted between VC0023/VC0024	This study
$crtS_{WT/VC2238}$	WT *with crtS* inserted between VC2237/VC2238	This study
$WT\text{-}_{EV}$	WT after ~200 generations (experimental evolution)	This study
D185	WTΔ*crtS* with 2 separate chromosomes (before experimental evolution)	This study

D185-$_{EV}$	D185 after ~200 generations (experimental evolution)	This study
D247	WTΔ*crtS* with 2 separate chromosomes (before experimental evolution)	This study
D247-$_{EV}$	D247 after ~200 generations (experimental evolution)	This study
C667	WTΔ*crtS* with 2 separate chromosomes (before experimental evolution)	This study
C667-$_{EV}$	C667 after ~200 generations (experimental evolution)	This study
C926	WTΔ*crtS* with single fused chromosomes (before experimental evolution)	This study
C926-$_{EV1}$	C926 after ~100 generations (experimental evolution)	This study
C926-$_{EV2}$	C926 after ~200 generations (experimental evolution)	This study
V. cholerae strains tagged for fluorescent microscopy		
WT [*ori1* - *ori2*]	WT ; [*parST1*@VC2759];[*lacO*@VCA1092];[*lacZ*::(*lacI-mCherry*,*parB1-yGFP*,*zeo*)]	This study
WT [VC783 - *ori2*]	WT ; [*parST1*@VC0783];[*lacO*@VCA1092];[*lacZ*::(*lacI-mCherry*,*parB1-yGFP*,*zeo*)]	This study
WT [*ter1* - *ter2*]	WT ; [*parST1*@VC1508];[*lacO*@VCA560];[*lacZ*::(*lacI-mCherry*,*parB1-yGFP*,*zeo*)]	This study
Δ*crtS* [VC783 - *ori2*]	WTΔ*crtS*#7 ; [*parST1*@VC0783];[*lacO*@VCA1092];[*lacZ*::(*lacI-mCherry*,*parB1-yGFP*,*zeo*)]	This study
crtS$_{VC23}$ [*ori1* - *ori2*]	crtS$_{VC23}$; [*parST1*@VC2759];[*lacO*@VCA1092];[*lacZ*::(*lacI-mCherry*,*parB1-yGFP*,*zeo*)]	This study
crtS$_{VC23}$ [VC783 - *ori2*]	crtS$_{VC23}$; [*parST1*@VC0783];[*lacO*@VCA1092];[*lacZ*::(*lacI-mCherry*,*parB1-yGFP*,*zeo*)]	This study
crtS$_{VC23}$ [*ter1* - *ter2*]	crtS$_{VC23}$; [*parST1*@VC1508];[*lacO*@VCA0560];[*lacZ*::(*lacI-mCherry*,*parB1-yGFP*,*zeo*)]	This study
crtS$_{WT/VC23}$ [*ori1* - *ori2*]	crtS$_{WT/VC23}$; [*parST1*@VC2759];[*lacO*@VCA1092];[*lacZ*::(*lacI-mCherry*,*parB1-yGFP*,*zeo*)]	This study
crtS$_{WT/VC2238}$ [*ori1* - *ori2*]	crtS$_{WT/VC2238}$; [*parST1*@VC2759];[*lacO*@VCA1092];[*lacZ*::(*lacI-mCherry*,*parB1-yGFP*,*zeo*)]	This study

table S3. Primers used in qPCR.

Name	Sequence (5'→3')	Target
ori1-Fwd	GATTCATTACGCCGCTTCTCCC	VC2775
ori1-Rev	TGAAGCTCAATGCGGCTAAACC	
ori2-Fwd	AGGCCTTCTCGGTATCCGTCTC	VCA0003
ori2-Rev	CTGCCGTCGCTGAATTACAACC	

SUPPLEMENTARY MOVIES

movie S1. 3D representations of the contact map from fig. S9 (exponential growth of WT in LB).

movie S2. 3D representations of the contact map from fig. S9 (exponential growth of WT in MM).

movie S3. Timelapse fluorescent microscopy of Δ*crtS* filamentous cells, tagged at VC783 (Chr1) and near *ori2* (Chr2), growing on a M9 minimal medium agar pad supplemented with fructose and thiamine. VC783 and *ori2* are visualized in green and red respectively.

movie S4. Timelapse fluorescent microscopy of Δ*crtS* filamentous cells, tagged at VC783 (Chr1) and near *ori2* (Chr2), growing on a M9 minimal medium agar pad supplemented with fructose and thiamine. VC783 and *ori2* are visualized in green and red respectively. Asterisks (*) indicate an event when cell division is giving rise to a Chr2-less cell which does not elongate nor divide.